

Li-Ion Transport and Solution Structure in Sulfolane-Based Localized High-Concentration Electrolytes

Published as part of *The Journal of Physical Chemistry virtual special issue "Research and Development of Novel Secondary Batteries in Japan"*.

Taku Sudoh,¹ Shuhei Ikeda,¹ Keisuke Shigenobu, Seiji Tsuzuki, Kaoru Dokko, Masayoshi Watanabe, Wataru Shinoda,* and Kazuhide Ueno*



Cite This: *J. Phys. Chem. C* 2023, 127, 12295–12303



Read Online

ACCESS |



Metrics & More

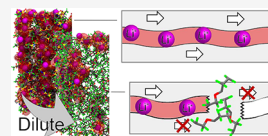


Article Recommendations



Supporting Information

ABSTRACT: Localized high-concentration electrolytes (LHCEs), which are mixtures of highly concentrated electrolytes (HCEs) and non-coordinating diluents, have attracted significant interest as promising liquid electrolytes for next-generation Li secondary batteries, owing to their various beneficial properties both in the bulk and at the electrode/electrolyte interface. We previously reported that the large Li⁺-ion transference number in sulfolane (SL)-based HCEs, attributed to the unique exchange/hopping-like Li⁺-ion conduction, decreased upon dilution with the non-coordinating hydrofluoroether (HFE) despite the retention of the local Li⁺-ion coordination structure. Therefore, in this study, we investigated the effects of HFE dilution on the Li⁺ transference number and the solution structure of SL-based LHCEs via the analysis of dynamic ion correlations and molecular dynamics simulations. The addition of HFE caused nano-segregation in the SL-based LHCEs to afford polar and nonpolar domains and fragmentation of the polar ion-conducting pathway into smaller clusters with increasing HFE content. Analysis of the dynamic ion correlations revealed that the anti-correlated Li⁺–Li⁺ motions were more pronounced upon HFE addition, suggesting that the Li⁺ exchange/hopping conduction is obstructed by the non-ion-conducting HFE-rich domains. Thus, the HFE addition affects the entire solution structure and ion transport without significantly affecting the local Li⁺-ion coordination structure. Further studies on ion transport in LHCEs would help obtain a design principle for liquid electrolytes with high ionic conductivity and large Li⁺-ion transference numbers.



1. INTRODUCTION

The development of high-energy-density and low-cost rechargeable batteries is important to realize a shift from fossil fuel sources to those of renewable energy.^{1,2} Electrolyte materials play a crucial role in realizing the practical applications of next-generation rechargeable batteries. Among the proposed electrolyte materials, highly concentrated electrolytes (HCEs) exhibit improved thermal and electrochemical stabilities as well as stable cycling of high-voltage positive electrodes and lithium metal negative electrodes.^{3–9} Moreover, we previously reported the unique exchange/hopping-like Li⁺-ion transport in sulfolane (SL)-based HCEs containing Li salts.¹⁰ In the SL-based HCEs, SL coordinates to two vicinal Li⁺ ions forming an SL- and anion-bridged, chain-like Li⁺ coordination structure, which contributed to the highly efficient Li⁺-ion transport; this has been evidenced by the rapid diffusion of Li⁺ ions compared to that of SL and the counter anions as well as a high Li⁺-ion transference number (0.7–0.8) under anion-blocking conditions.^{10–12} Furthermore, the SL-based HCEs demonstrated an improved rate performance in Li-ion batteries and Li–S batteries.^{10,12,13}

However, HCEs demonstrate low ionic conductivity and poor electrode wettability due to their significantly high viscosity. Previous studies have reported that the dilution of

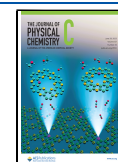
HCEs with a low-polarity solvent such as hydrofluoroethers enhanced the ionic conductivity and wettability without losing the merits of the electrochemical characteristics of the parent HCEs.^{14–16} For instance, the addition of 1,1,2,2-tetrafluoroethyl-2,2,3,3-tetrafluoropropyl ether (HFE) to a 1:1 molar mixture of Li[TFSA] and tetraglyme (G4) ([Li(G4)][TFSA]) improved the viscosity and conductivity to the same level as those of typical 1 mol dm^{−3} organic electrolyte solutions.¹⁶ This electrolyte design has been termed as localized high-concentration electrolytes (LHCEs) and is widely applied to electrolyte materials in lithium batteries.^{17–19}

Considerable efforts have also been invested in elucidating the ion-transport mechanism in HCEs based on concentrated-electrolyte theory.^{20–25} We previously studied the effects of diluents on the dynamic ion correlation in diluted [Li(G4)][TFSA] based on Roling and Bedrov's concentrated-solution theory.²⁶ The addition of non-coordinating HFE did not alter

Received: March 30, 2023

Revised: May 12, 2023

Published: June 20, 2023



the ion-transport mechanism in [Li(G4)][TFSA], resulting in an unchanged Li^+ -ion transference number and increased ionic conductivity. A similar phenomenon, where the high Li^+ transference number is retained and the ionic conductivity is improved, was expected when SL-based HCEs are diluted with non-coordinating HFE. However, in practice, the Li^+ transference number decreased.^{12,13,27} This could be attributed to the reduced contribution of the Li^+ exchange/hopping mechanism to the ionic conduction; however, the practical changes in the ion-transport mechanism and Li^+ -ion coordination structure remained unclear. Therefore, in this study, we investigated the dilution effect on the Li^+ transference number and Li-ion coordination structure in SL-based LHCEs. In this study, HFE was used as the diluent for SL-based LHCEs owing to the miscibility with [Li(SL)₂]-[TFSA], non-flammability, and a relatively high boiling point. In addition, the concentration dependence of the dynamic ion correlation in diluted SL-based HCEs was studied in a similar manner to that of diluted [Li(G4)][TFSA] in a previous report.²⁶ We also performed all-atom molecular dynamics (MD) simulations to validate the changes in the solution structure and its relation to the ion-transport mechanism in SL-based LHCEs.

2. EXPERIMENTAL SECTION

2.1. Materials. Triglyme (G3, battery grade, water content <50 ppm), SL (battery grade, water content <50 ppm), and lithium bis(trifluoromethanesulfonyl)amide (LiTFSA, purity >99.9%, water content <100 ppm) were purchased from Kishida Chemical Co., Ltd. (Japan). 1,1,2,2-Tetrafluoroethyl-2,2,3,3-tetrafluoropropyl ether (HFE) was purchased from Daikin Industries Ltd. (Japan). These purified solvents and the Li salt were used as received. The SL-based HCE [Li(SL)₂]-[TFSA] was prepared by mixing LiTFSA and SL in the appropriate molar ratios. [Li(SL)₂][TFSA]-*x*HFE was prepared by mixing the stoichiometric Li salt and solvent in a 1:2 ratio and diluting with HFE in the appropriate molar ratios of *x*. All electrolyte preparations were performed in an inert argon-filled glovebox ($[\text{H}_2\text{O}] < 1 \text{ ppm}$, $[\text{O}_2] < 1 \text{ ppm}$).

2.2. Measurements. The self-diffusion coefficients of Li ($D_{\text{Li}}^{\text{self}}$), TFSA ($D_{\text{TFSA}}^{\text{self}}$), and the solvents ($D_{\text{SL}}^{\text{self}}$ and $D_{\text{HFE}}^{\text{self}}$) were determined within an error of 10% using pulse-field-gradient (PFG) nuclear magnetic resonance (NMR), as that in our previous report.²⁶ A JEOL ECX-400 NMR spectrometer with a 9.4 T narrow-bore superconducting magnet and a PFG probe was used for the measurements. PFG (*g*) was calibrated using deuterated water. ¹H, ⁷Li, and ¹⁹F NMR spectra were recorded for the solvents, Li, and TFSA, respectively. Raman spectra were recorded using a 532 nm laser Raman spectrometer (NRS-4100, JASCO) at a resolution of $\sim 4 \text{ cm}^{-1}$ and calibrated using a polypropylene standard. The temperature of the samples was regulated at 30 °C using a Peltier microscope stage (TS62, INSTEC) with a temperature controller (mk1000, INSTEC). Two different Li^+ transference numbers ($t_{\text{Li}}^{\text{NMR}}$ and $t_{\text{Li}}^{\text{EC}}$) were estimated based on previous reports.^{26,28} The value of $t_{\text{Li}}^{\text{EC}}$ was determined using Li/Li symmetric cells encapsulated in 2032-type coin cells. A porous glass filter paper (Advantec, GA55, diameter = 17 mm) soaked with the electrolytes was placed between two Li foil electrodes (Honjo Metal, diameter = 16 mm). Before potentiostatic polarization, the electrochemical impedance measurements were performed every hour in the frequency range of 0.1 Hz–1 MHz at an alternating voltage amplitude of 5 or 10 mV, using a ModuLab

XM ECS electrochemical test system (Solartron Analytical). This confirmed the interfacial stabilization of the Li electrodes. After stabilization of the cells, a polarization curve with a potential step of 5 or 10 mV was obtained until the current reached a steady state. Subsequently, electrochemical impedance spectra were recorded to obtain the interfacial impedance of the polarized cells. Ionic conductivity (σ_{ion}) was obtained using a complex impedance method in the frequency range of 1 Hz–500 kHz at an alternating voltage amplitude of 10 mV (VMP3, Biologic). The cell constants of the conductivity cells (two platinum black electrode cells) were determined using a 0.01 mol dm⁻³ KCl aqueous solution at 25 °C. Ionicity, defined as the molar conductivity fraction ($\Lambda_{\text{imp}}/\Lambda_{\text{NMR}}$), is estimated to obtain information about the degree of dissociation, where Λ_{imp} is the experimental molar conductivity and Λ_{NMR} is obtained from the self-diffusion coefficients of the ions using the Nernst–Einstein equation, $\Lambda_{\text{NMR}} = F^2(D_{\text{Li}}^{\text{self}} + D_{\text{anion}}^{\text{self}})/RT$, where *F* is the Faraday constant, *R* is the gas constant, and *T* is the absolute temperature. The densities and viscosities were simultaneously measured using a Stabinger viscometer (SVM300, Anton Paar).

The following measurements were performed to calculate the Onsager transport coefficients.^{22,25,29} The salt diffusion coefficients (D_{salt}) of electrolytes were determined using Li/Li symmetric cells, which were polarized at a constant current density of 0.25 mA cm⁻² until a steady state was reached. The voltage relaxation of the cell potential was recorded after the applied current was removed. The electrode potential of Li/Li⁺ (electromotive force, EMF) in each electrolyte was measured with respect to the reference electrode, Li/Li⁺ in 1 mol dm⁻³ LiTFSA/G3, using a multi-compartment concentration cell, in which Vycor glass was used for the junction between the reference and sample electrolytes. The value of $d\phi/d\ln(c)$ at a given concentration was obtained from the slope of the plot of Li-salt concentration vs potential, as shown in Figure S1. To determine the concentration dependence of the EMF of [Li(SL)₂][TFSA]-*x*HFE, the Li-salt concentration was varied by changing the amount of SL while maintaining the molar ratios of Li[TFSA] and HFE, assuming concentration polarization in the electrochemical cells. All the above experimental cells were prepared and sealed in the glovebox, and the measurements were performed at 30 °C unless otherwise noted.

2.3. Dynamic Ion Correlations. To evaluate the dynamic ion correlations, the Onsager transport coefficients were determined from the experimental transport data, σ_{ion} , $t_{\text{Li}}^{\text{EC}}$, D_{salt} , $D_{\text{Li}}^{\text{self}}$, $D_{\text{anion}}^{\text{self}}$, and $d\phi/d\ln(c)$, for a given electrolyte based on Roling and Bedrov's concentrated-electrolyte theory.^{22,25} The experimental transport data are listed in Table S1. The Onsager transport coefficients were expressed as the fraction of the contribution to the total ionic conductivity (σ_{ion}) as shown below:

$$\sigma_{\text{ion}} = \sigma_{++} + \sigma_{--} - 2\sigma_{+-} \quad (1)$$

The transport coefficients for the cation (σ_{++}) and the anion (σ_{--}) obtained from eqs S1 ~ S7 in the Supporting Information can be divided into self-terms and distinct terms, and σ_{ion} was rewritten as follows:

$$\sigma_{\text{ion}} = \sigma_{+}^{\text{self}} + \sigma_{++}^{\text{distinct}} + \sigma_{-}^{\text{self}} + \sigma_{--}^{\text{distinct}} - 2\sigma_{+-} \quad (2)$$

The self-terms σ_{+}^{self} and σ_{-}^{self} were estimated using the Nernst–Einstein equation as follows:

$$\sigma^{\text{self}} = \frac{cF^2}{RT} D^{\text{self}} \quad (3)$$

In addition, the distinct terms $\sigma_{++}^{\text{distinct}}$ and $\sigma_{--}^{\text{distinct}}$ can be estimated by subtracting σ_{+}^{self} and σ_{-}^{self} from σ_{++} and σ_{--} , respectively. The positive and negative signs of the distinct terms indicate correlated and anti-correlated ion motions, respectively. The numerical data are listed in Table S2, and the procedure for calculating the Onsager transport coefficients under anion-blocking conditions has been adopted from a previously reported method.²²

2.4. MD Simulations. MD simulations using a polarizable force field were performed using the polarizable version of MPDYN simulation software.³⁰ Previously reported OPLS-AA-based force-field parameters for SL and LiTFSA were used to model the polarizable force fields.³¹ New parameters were developed for HFE based on ab initio molecular orbital calculations. The details for the polarizable force fields are provided in Figure S2 and Tables S3–S7. The initial structures of the electrolytes were prepared using the PACKMOL code.³² Production simulations of the mixtures of SL, LiTFSA, and HFE were conducted in the NPT ensemble. The pressure and temperature were maintained at 0.1 MPa and 363 K using an Andersen barostat³³ and a Nosé–Hoover chain thermostat,³⁴ respectively. All the C–H bonds were held rigid using the SHAKE algorithm.³⁵ Reversible RESPA was used for multiple-time step integration of equations for the motion of atoms.^{36,37} Periodic boundary conditions were employed. The nonbonded forces were truncated at 12 Å, while the Coulomb interactions were computed using the Ewald method.³⁸ The time step size for updating interactions in the Ewald reciprocal space was 8 fs and that for other interactions was 2 fs. The production run was conducted for 100 ns, and the trajectories were used for various analyses.

The radial distribution function and accumulative coordination number of oxygen atoms around Li⁺ ions were calculated to investigate the solution structure of the electrolytes. The radial distribution function, $g_j(r)$, of the j -th segment around the i -th segment was calculated as follows:

$$g_{ij}(r) = \frac{1}{4\pi r^2 \Delta r} \frac{V}{N_j} \langle \Delta n_{ij}(r) \rangle \quad (4)$$

where $\langle \Delta n_{ij}(r) \rangle$ is the average number of j -th segments found at a distance of r from the i -th segment, and the grid size of Δr was set to 0.1 Å. The accumulative coordination number was calculated as follows:

$$N_{ij}(r) = \int_0^r \langle \Delta n_{ij}(r) \rangle dr \quad (5)$$

3. RESULTS AND DISCUSSION

3.1. Transport Properties of [Li(SL)₂][TFSA]-xHFE. As shown in Figure 1a, the addition of HFE to [Li(SL)₂][TFSA] caused two orders of magnitude increase in the self-diffusion coefficients of the ions at the lowest salt concentration (c) of 0.18 mol dm⁻³ ($x = 35$) and significantly decreased the viscosity of the electrolyte.¹² However, the increase in conductivity was less significant than that expected from an increase in the self-diffusion coefficients: the conductivity (σ_{ion}) increased by a factor of 2.1 from 0.42 mS cm⁻¹ for the non-diluted HCE ($x = 0$) to a maximum value of 0.90 mS

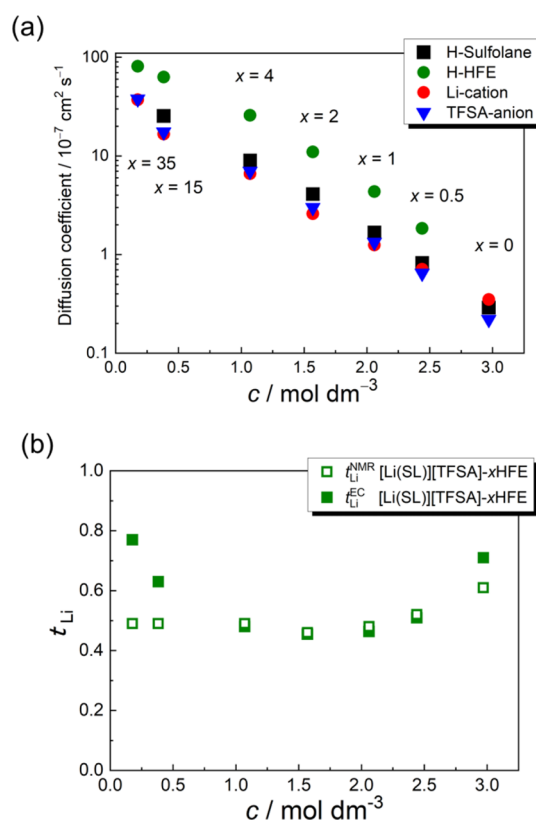


Figure 1. Concentration dependence of (a) self-diffusion coefficients and (b) Li⁺ transference numbers ($t_{\text{Li}}^{\text{FC}}$ and $t_{\text{Li}}^{\text{NMR}}$) of [Li(SL)₂]-[TFSA]- x HFE electrolytes at 30 °C. Abbreviations: SL, sulfolane; TFSA, bis(trifluoromethanesulfonyl)amide; HFE, hydrofluoroether.

cm⁻¹ for the LHCE at a c of 1.57 mol dm⁻³ ($x = 2$) (see the Supporting Information, Table S1).¹²

First, we focused on the order of the self-diffusion coefficients of the components in the SL-based HCE and LHCEs in the c range of 0.38–2.97 mol dm⁻³ to elucidate the changes in the Li-ion transport upon dilution with HFE. At $c = 2.97$ mol dm⁻³, the self-diffusion coefficient of Li ($D_{\text{Li}}^{\text{self}}$) was higher than those of the other species ($D_{\text{TFSA}}^{\text{self}}$ and $D_{\text{SL}}^{\text{self}}$) in the non-diluted [Li(SL)₂][TFSA]. This diffusion behavior is anomalous and cannot be interpreted by simple translational diffusion of the solvated Li⁺ ions observed in typical organic electrolyte solutions.³⁹ A previous Raman study combined with X-ray crystallography¹² revealed that each Li⁺ ion is linked to two neighboring SLs, forming a –SL–Li⁺–SL– chain-like Li⁺-ion coordination in the HCEs. Furthermore, TFSA⁻ would form –TFSA⁻–Li⁺–TFSA⁻– aggregated ion pairs with Li⁺ ions. Such chain-like Li⁺-ion coordination structures in the HCEs cause efficient Li⁺-ion exchange between the coordinating/vacant sites without dragging the solvent and anion molecules. This explains the unusual Li⁺-ion diffusion behavior in SL-based HCEs. However, even a small addition of HFE to [Li(SL)₂][TFSA] changed the order of the self-diffusion coefficients of the components. At $c = 2.44$ mol dm⁻³, $D_{\text{Li}}^{\text{self}}$ was smaller than $D_{\text{SL}}^{\text{self}}$, whereas $D_{\text{Li}}^{\text{self}}$ was slightly larger than $D_{\text{TFSA}}^{\text{self}}$. However, in the c_{Li} range lower than 2.06 mol dm⁻³, $D_{\text{Li}}^{\text{self}}$ was comparable to $D_{\text{TFSA}}^{\text{self}}$, and the diffusion coefficients were in the order of $D_{\text{HFE}}^{\text{self}} > D_{\text{SL}}^{\text{self}} > D_{\text{Li}}^{\text{self}} \sim D_{\text{TFSA}}^{\text{self}}$. The rapid diffusion of HFE is characteristic of its non-coordinating property, as evidenced by the solvent parameters (permittivity $\epsilon = 6.7$ and Gutmann's donor number DN = 1.9).¹⁶ Furthermore, $D_{\text{SL}}^{\text{self}} >$

$D_{\text{Li}}^{\text{self}}$ suggests the liberation of SL molecules from the unique coordination structures in the LHCEs. The observed change in the order of the diffusion coefficients is attributed to the changes in the solution structure and conduction mechanism in the absence and presence of HFE.

The Li^+ transference number in the SL-based LHCEs was evaluated to further elucidate the changes in the Li -ion transport. Several methods have been proposed for estimating the Li^+ transference number of the electrolytes in the literature.²⁸ In a previous report on glyme-based LHCEs,²⁶ Li^+ transference numbers were estimated via two different methods: one was derived from PFG-NMR ($t_{\text{Li}}^{\text{NMR}}$) and another was estimated electrochemically ($t_{\text{Li}}^{\text{EC}}$) using the Bruce–Vincent and Watanabe method.^{40,41} In this study, $t_{\text{Li}}^{\text{NMR}}$ was defined as the proportion of the self-diffusion coefficient of Li^+ ($D_{\text{Li}}^{\text{self}}$) in the summation of the coefficients of the ion species $D_{\text{Li}}^{\text{self}}$ and $D_{\text{TFSA}}^{\text{self}}$ as shown below:

$$t_{\text{Li}}^{\text{NMR}} = \frac{D_{\text{Li}}^{\text{self}}}{D_{\text{Li}}^{\text{self}} + D_{\text{TFSA}}^{\text{self}}} \quad (6)$$

In addition, $t_{\text{Li}}^{\text{EC}}$ was defined as the ratio of the steady-state current to the initial current with a correction for interfacial impedance contributions, as shown below:

$$t_{\text{Li}}^{\text{EC}} = \frac{I_{\text{SS}}(V_{\text{DC}} - I_{\text{Ohm}}R_{i,0})}{I_{\text{Ohm}}(V_{\text{DC}} - I_{\text{SS}}R_{i,\text{SS}})} \quad (7)$$

where I_{Ohm} and I_{SS} are the initial and steady-state currents, respectively. I_{Ohm} was calculated based on Ohm's law: $I_{\text{Ohm}} = V_{\text{DC}}/(R_{\text{bulk}} + R_{i,0})$, where V_{DC} is the applied voltage, and $R_{i,0}$ and $R_{i,\text{SS}}$ are the initial and steady-state interfacial resistances, respectively.

In an ideal electrolyte solution at infinite dilutions, both $t_{\text{Li}}^{\text{NMR}}$ and $t_{\text{Li}}^{\text{EC}}$ would become equivalent to the true Li^+ transference number; however, they will differ from each other in non-ideal electrolyte solutions. In addition, $t_{\text{Li}}^{\text{NMR}}$ is estimated from the self-diffusion coefficient of an individual ion; therefore, the effects of strong ion–ion interactions and correlations in HCEs are ignored. In contrast, $t_{\text{Li}}^{\text{EC}}$ is measured in an electrochemical cell under anion-blocking conditions and can be defined as the current fraction of migrated and diffused Li^+ ions. Thus, it can deviate from the true value in HCEs but is an efficient parameter to characterize the transport properties of battery electrolytes. For the Li^+ -ion conductivity ($\sigma_{\text{ion}} \times t_{\text{Li}}^{\text{EC}}$), the highest value was obtained at $c = 1.57 \text{ mol dm}^{-3}$ (Table S1). Unlike $t_{\text{Li}}^{\text{NMR}}$, $t_{\text{Li}}^{\text{EC}}$ is strongly affected by dynamic ion correlations as well as salt diffusion. Moreover, a previous study reported a large difference between $t_{\text{Li}}^{\text{NMR}}$ (0.5) and $t_{\text{Li}}^{\text{EC}}$ (0.03) for $[\text{Li}(\text{G4})][\text{TFSA}]$.^{11,29} Although dynamic ion correlations have not been considered for $t_{\text{Li}}^{\text{NMR}}$, significant anti-correlated $\text{Li}^+ - \text{Li}^+$ and $\text{Li}^+ - \text{TFSA}^-$ motions of the long-lived $[\text{Li}(\text{G4})]^+$ cation and the bulky TFSA^- anion were considered responsible for the extremely low $t_{\text{Li}}^{\text{EC}}$ under the constraint of momentum conservation.

Figure 1b shows the Li -salt concentration dependence of Li^+ transference numbers ($t_{\text{Li}}^{\text{NMR}}$ and $t_{\text{Li}}^{\text{EC}}$) in the $[\text{Li}(\text{SL})_2][\text{TFSA}]$ - x HFE electrolytes. Both $t_{\text{Li}}^{\text{NMR}}$ and $t_{\text{Li}}^{\text{EC}}$ exceeded 0.6 in the non-diluted $[\text{Li}(\text{SL})_2][\text{TFSA}]$ ($c = 2.97 \text{ mol dm}^{-3}$). However, both values monotonically decreased to ~ 0.5 at an HFE dilution of $c = 1.57 \text{ mol dm}^{-3}$. In the low c range of $0.38 - 1.57 \text{ mol dm}^{-3}$, $t_{\text{Li}}^{\text{EC}}$ increased with further addition of HFE, whereas $t_{\text{Li}}^{\text{NMR}}$ remained nearly constant at ~ 0.5 . For the non-diluted

$[\text{Li}(\text{SL})_2][\text{TFSA}]$, a positive effect of the dynamic ion correlations on the Li^+ -ion conduction would result in a larger $t_{\text{Li}}^{\text{EC}}$ than $t_{\text{Li}}^{\text{NMR}}$. This is because the Li^+ -ion exchange/hopping conduction through the chain-like Li^+ -ion coordination structures would not only allow a larger $D_{\text{Li}}^{\text{self}}$ but also alleviate the strongly anti-correlated ion motions in highly concentrated systems.¹¹ In the c range of $1.57 - 2.44 \text{ mol dm}^{-3}$, the differences in $t_{\text{Li}}^{\text{NMR}}$ and $t_{\text{Li}}^{\text{EC}}$ are insignificant, suggesting that the dynamic ion correlations are less affected in this concentration region. In contrast, the deviation between $t_{\text{Li}}^{\text{EC}}$ and $t_{\text{Li}}^{\text{NMR}}$ gradually increased in the highly diluted region ($c \leq 1.07 \text{ mol dm}^{-3}$). This is not expected for ideal electrolyte solutions where $t_{\text{Li}}^{\text{EC}} = t_{\text{Li}}^{\text{NMR}}$ at infinite dilutions, which suggests that the SL-based LHCEs behaved as a non-ideal electrolyte. The obvious deviation between $t_{\text{Li}}^{\text{EC}}$ and $t_{\text{Li}}^{\text{NMR}}$ further implies that the effect of the unique Li^+ -ion exchange/hopping conduction on dynamic ion correlations was attenuated in the presence of a large amount of HFE.

Onsager transport coefficients were experimentally estimated based on concentrated-solution theory to elucidate the dynamic ion correlations for the $[\text{Li}(\text{SL})_2][\text{TFSA}]$ - x HFE electrolytes. Figure 2a shows the concentration dependence

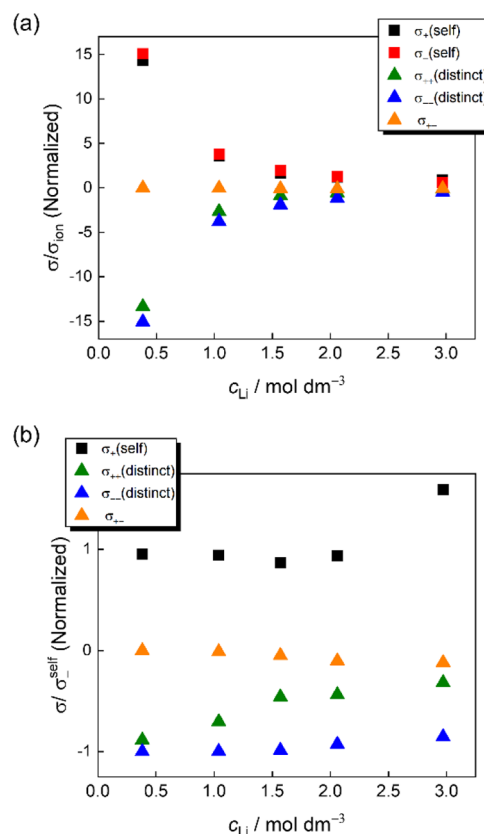


Figure 2. Concentration dependence of the normalized transport coefficients (a) $\sigma / \sigma_{\text{ion}}$ and (b) $\sigma / \sigma_{\text{ion}}^{\text{self}}$ of the SL-based LHCEs.

of the normalized transport coefficients ($\sigma / \sigma_{\text{ion}}$) for $[\text{Li}(\text{SL})_2][\text{TFSA}]$ - x HFE. Both $\sigma_+^{\text{self}} / \sigma_{\text{ion}}$ and $\sigma_-^{\text{self}} / \sigma_{\text{ion}}$ increased significantly with the addition of HFE to $[\text{Li}(\text{SL})_2][\text{TFSA}]$. These ratios exceeded unity in the SL-based LHCEs and were ~ 15 at $c = 0.38 \text{ mol dm}^{-3}$. This clearly shows that the contribution of $D_{\text{Li}}^{\text{self}}$ and $D_{\text{TFSA}}^{\text{self}}$ to the ionic conductivity (σ_{ion}) was small, where σ_+^{self} and σ_-^{self} were estimated using eq 3. In practice, $D_{\text{Li}}^{\text{self}}$ and $D_{\text{TFSA}}^{\text{self}}$ could have an average value that includes those of

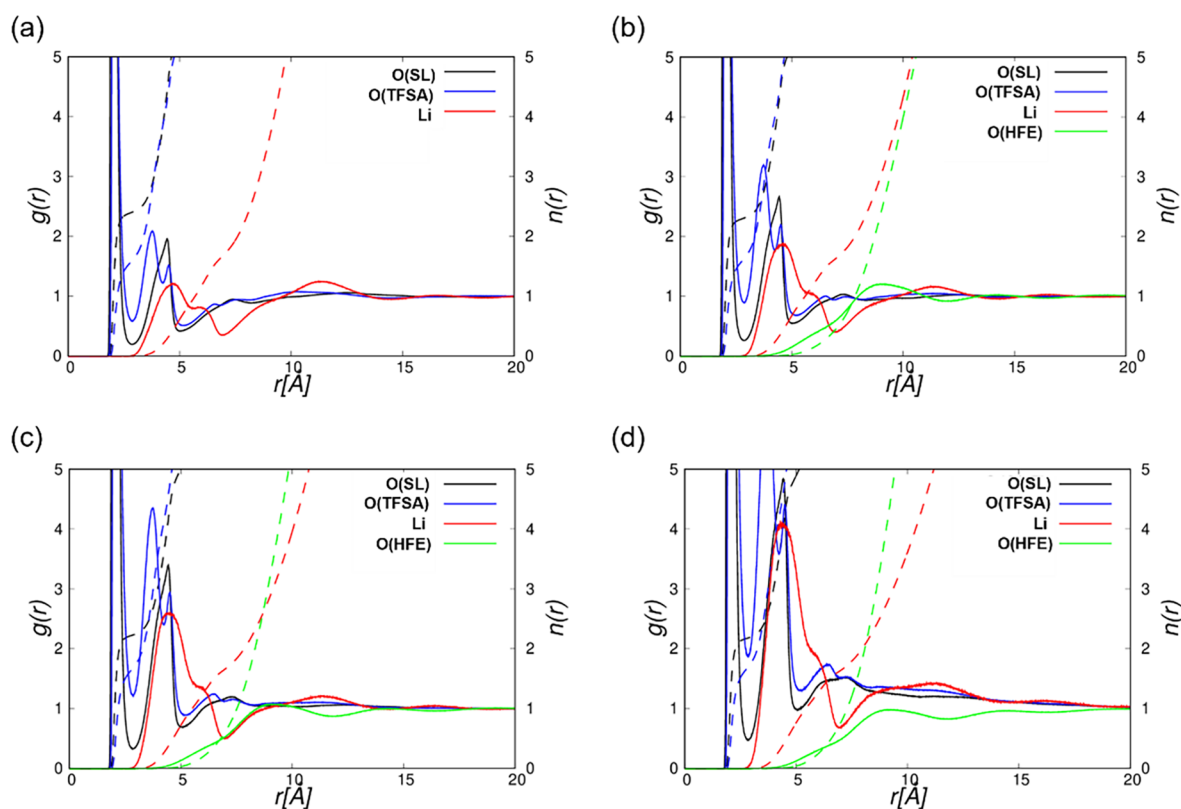


Figure 3. Radial distribution functions g around Li^+ ions and accumulative coordination numbers n of $\text{Li}-\text{O}(\text{SL})$, $\text{Li}-\text{O}(\text{TFSA})$, $\text{Li}-\text{Li}$, and $\text{Li}-\text{O}(\text{HFE})$ for (a) SL-based HCEs and LHCEs at a salt concentration (c) of (b) 2.06, (c) 1.57, and (d) 1.07 mol dm^{-3} .

neutral ion pairs or aggregates as well as fully dissociated ions. In addition, ionicity ($\Lambda_{\text{imp}}/\Lambda_{\text{NMR}}$), which is relevant to the apparent degree of dissociation or dynamic ion correlations in electrolyte solutions,³⁹ drastically reduced with the addition of HFE (Figure S3). Therefore, the significantly large values of $\sigma_+^{\text{self}}/\sigma_{\text{ion}}$ and $\sigma_-^{\text{self}}/\sigma_{\text{ion}}$ are attributed to the presence of neutral ion pairs or aggregates in non-ideal electrolyte solutions such as $[\text{Li}(\text{SL})_2][\text{TFSA}]\cdot x\text{HFE}$. Moreover, $\sigma_{++}^{\text{distinct}}/\sigma_{\text{ion}}$ and $\sigma_{--}^{\text{distinct}}/\sigma_{\text{ion}}$ had negative values, which do not properly reflect the actual change in the dynamic ion correlations of $[\text{Li}(\text{SL})_2][\text{TFSA}]\cdot x\text{HFE}$.

To highlight the degree of variation in the cross-correlated ion–ion motions upon dilution with HFE, the transport coefficients were normalized using σ_-^{self} (Figure 2b). $\sigma_{--}^{\text{distinct}}/\sigma_-^{\text{self}}$ does not change significantly and remains a negative value even with the addition of HFE. However, $\sigma_{+-}/\sigma_-^{\text{self}}$ increased with the addition of HFE, which could be attributed to the enhanced interaction between Li^+ and TFSA^- in the presence of the low-permittivity HFE. Previously, the HCEs comprising strongly Lewis basic anions such as BF_4^- and CF_3SO_3^- were observed to exhibit a larger $t_{\text{Li}}^{\text{EC}}$ compared to the HCEs comprising TFSA^- .⁴² Therefore, the enhanced interaction between Li^+ and TFSA^- would contribute to the increase in the $t_{\text{Li}}^{\text{EC}}$ of the LHCEs in the low c range of 0.38–1.57 mol dm^{-3} (Figure 1b). Notably, upon the addition of HFE, $\sigma_{++}^{\text{distinct}}/\sigma_-^{\text{self}}$ significantly decreased in the low c range, whereas it slightly decreased in the c range of 1.57–2.97 mol dm^{-3} . Moreover, the Li^+ -ion exchange/hopping conduction mechanism could also be involved in the insignificant anti-correlations in the higher c range, even in the LHCEs. However, the value of $\sigma_{++}^{\text{distinct}}/\sigma_-^{\text{self}}$ decreased in the lower c range, suggesting that the excessive addition of HFE diminishes the unique Li^+ -ion

exchange/hopping conduction and enhances the anti-correlated Li^+-Li^+ motions. In addition, the decrease in the ionic conductivity owing to the anti-correlated Li^+-Li^+ and $\text{TFSA}^--\text{TFSA}^-$ motions in the low c region is less than that expected from an increase in ionic diffusivity.¹² In Figure S4, the values of $\sigma_{++}^{\text{distinct}}/\sigma_-^{\text{self}}$ are plotted against the volume fraction (ϕ) of $[\text{Li}(\text{SL})_2][\text{TFSA}]$ in the LHCEs. The volume molar volume of each electrolyte was calculated using the density and mole fraction of the electrolytes and converted to ϕ . A clear decline of $\sigma_{++}^{\text{distinct}}/\sigma_-^{\text{self}}$ was observed at a ϕ of ~ 0.5 ($c = 1.57 \text{ mol dm}^{-3}$). Although the SL-based LHCEs are macroscopically homogeneous solutions, $[\text{Li}(\text{SL})_2][\text{TFSA}]$ and the non-coordinating HFE can be nano-segregated at a molecular level similar to other HCEs reported in the literature.^{43–46} Therefore, the ion-conducting $[\text{Li}(\text{SL})_2][\text{TFSA}]$ phase may be partially isolated in the sea of HFE in a ϕ range lower than 0.5, and the Li^+ exchange/hopping conduction is obstructed by the non-ion-conducting HFE-rich domains.²⁷

3.2. Solution Structure of $[\text{Li}(\text{SL})_2][\text{TFSA}]\cdot x\text{HFE}$. To clarify the detailed solution structures in the SL-based LHCEs, MD simulations were performed using a polarizable force field. Figures 3 and S5 show the radial distribution functions, g , and accumulative coordination numbers around Li^+ ions, n , in the SL-based HCE and LHCEs, respectively. The first sharp peaks were observed at $\sim 2.0 \text{ \AA}$ for $\text{Li}-\text{O}(\text{SL})$ and $\text{Li}-\text{O}(\text{TFSA})$ pair correlation functions for both HCE and LHCEs. The coordination number of oxygens to Li^+ ions within the first coordination shell, n^* , is well defined by the n value at the first minimum of g , which is $\sim 3.0 \text{ \AA}$. In addition, the $-\text{SL}-\text{Li}^+-\text{SL}-$ and $-\text{TFSA}-\text{Li}^+-\text{TFSA}-$ chain-like coordination structures were reflected by the second peaks for $\text{Li}-\text{O}(\text{SL})$ and $\text{Li}-\text{O}(\text{TFSA})$ and the first peaks for $\text{Li}-\text{Li}$ pair correlation

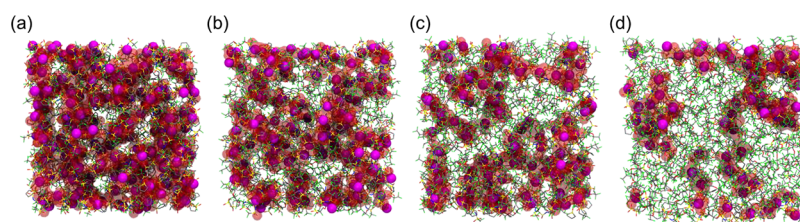


Figure 4. Snapshots of the MD simulations of (a) SL-based HCEs and those of LHCEs at a c of (b) 2.06, (c) 1.57, and (d) 1.07 mol dm⁻³. Color code: purple, lithium ion; gray, carbon; red, oxygen; yellow, sulfur; blue, nitrogen; green, fluorine. The red transparent volume represents the surface of oxygen atoms in the first coordination shell of Li⁺ ions.

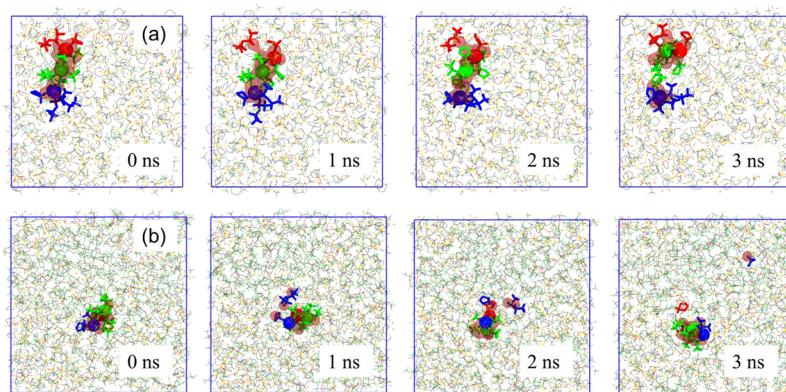


Figure 5. Snapshots of the time course of the MD simulations for (a) SL-based HCE and (b) LHCE at $c = 1.57$ mol dm⁻³. Li⁺ ions are represented by van der Waals spheres. Three Li⁺ ions were color-coded as red, blue, and green. SL and TFSA coordinated to the selected Li⁺ ions at the reference time of 0 ns are in the same color as the coordinating Li⁺ ion, respectively.

functions at ~ 5 Å. The intensity of these peaks increased with the addition of HFE, indicating that SL and TFSA⁻ locally condensed around Li⁺ ions against the average densities in the LHCEs. A broad peak for Li–O(HFE) first appeared at ~ 8 Å. These results confirm that HFE is not coordinated to Li⁺ ions, indicating the formation of the LHCE structure in the [Li(SL)₂][TFSA]-*x*HFE electrolytes.

Table S8 summarizes n^* values for SL and TFSA⁻ in each electrolyte. Although the total coordination number remains constant at ~ 4 in each electrolyte, the proportion of the molecules in the first solvation shell slightly changed with HFE dilution. For example, upon the dilution of the parent HCE with HFE to afford an LHCE at $c = 1.07$ mol dm⁻³, the n^* value decreased from 2.4 to 2.2 for SL and increased from 1.6 to 1.7 for TFSA⁻. The increased coordination number of TFSA⁻ is indicative of the enhanced Li⁺–TFSA⁻ interaction in the presence of HFE, which is consistent with the increased $\sigma_{+-}^{\text{distinct}}/\sigma_{-}^{\text{self}}$ (Figure 2b). This is also in good agreement with the Raman spectra (Figure S6). The strong band at 740–750 cm⁻¹ is ascribed to the S–N symmetric stretching vibration, and the CF₃ bending for TFSA⁻ shifted to a higher frequency, suggesting enhanced Li⁺–TFSA⁻ interaction and the consequent formation of contact ion pairs and aggregates.^{47–49} The slight decrease in the n^* for SL is attributed to the weakened Li⁺–SL interaction in the presence of HFE, which is supported by the experimental diffusivity data: $D_{\text{SL}}^{\text{self}} > D_{\text{Li}^+}^{\text{self}}$. Consequently, the confinement of [Li(SL)₂][TFSA] in the low-permittivity HFE resulted in enhanced Li⁺–TFSA⁻ interaction, which causes the partial replacement of the Li⁺-ion coordination of SL by TFSA⁻ in the LHCEs.

Figure 4 shows the snapshots of the MD simulations for the SL-based HCE and LHCEs. The red transparent region in Figure 4 represents the surface of the oxygen atoms of SL and

TFSA⁻ coordinated to Li⁺ ions. The surface was depicted by the surface representation of VMD software⁵⁰ with a probe radius of 1.4 Å. In the non-diluted [Li(SL)₂][TFSA] (Figure 4a), the coordination shells are interconnected to form a percolation network via the –SL–Li⁺–SL– and –TFSA–Li⁺–TFSA– chain-like coordination structures. In contrast, the non-highlighted region in the snapshot consists predominantly of less polar tetramethylene groups of SL. The observed polar–nonpolar domain structure in the HCEs is attributed to the amphiphilic property of SL toward Li⁺ ions.

As shown in Figure 4b–d, the snapshots clearly illustrate the nano-segregated solution structure of the [Li(SL)₂][TFSA]-*x*HFE electrolytes, that is, the LHCE structure with polar and nonpolar bi-continuous domains. The domain size of the non-highlighted region became larger with the addition of HFE, as the non-coordinating HFE molecules are soluble in the nonpolar domains of [Li(SL)₂][TFSA]. The polar domains (represented by the red transparent region) served as the ion-conducting path and are gradually fragmented into smaller clusters with increasing HFE content. However, the ion-conducting domains retained a continuous pathway in a c range higher than 1.57 mol dm⁻³ (Figure 4b,c), whereas they were isolated in the low c range of 1.07 mol dm⁻³ (Figure 4d). The fragmentation of the ion-conducting pathway observed in the MD simulations is closely linked to the observed changes in $\sigma_{++}^{\text{distinct}}/\sigma_{-}^{\text{self}}$ (Figure 2b) with the addition of HFE. From these results, we can conclude that the Li⁺ exchange/hopping conduction in the SL-based HCEs that suppressed the anti-correlated Li⁺–Li⁺ motion was obstructed by the non-ion-conducting HFE-rich domains.

Figure 5 shows the time course of the solution structure for the SL-based HCE and LHCE at $c = 1.57$ mol dm⁻³ in the MD simulations. The three neighboring Li⁺ ions that were present

at the reference time (0 ns) are displayed as red, blue, and green spheres, and SL and TFSA⁻ that were initially coordinated to the respective Li⁺ ions are shown in the same color. In the HCE (Figure 5a), the initial configuration of the three interconnected Li⁺ ions was relatively maintained even after 3 ns. Therefore, the slow dynamics of this unique coordination structure plays a crucial role in Li⁺-ion conduction. After 1 ns, the red Li⁺ ion, which was initially coordinated to TFSA⁻ (red), was liberated from the first coordination shell. However, TFSA⁻ (red) did not diffuse far from its initial position and coordinated to a different Li⁺ ion within 3 ns. At 3 ns, the green Li⁺ ion moved to a neighboring site, where the red Li⁺ ion was originally bound. These MD simulations clearly demonstrate the Li⁺-ion exchange/hopping conduction in the HCEs. Li⁺ ions were likely transferred independently within the chain-like coordination structure via the exchange/hopping mechanism, enabling faster Li⁺-ion diffusion relative to the other components and resulting in a high Li⁺ transference number.

For the LHCE at $c = 1.57 \text{ mol dm}^{-3}$ (Figure 5b), the unique coordination structure in the initial configuration (0 ns) was relatively maintained at 1 ns similar to that observed for the HCE. However, at 2 ns, both SL (blue) and TFSA⁻ (blue) moved from their respective Li⁺ ions. At 3 ns, SL (blue) was located far from the initial position. This is attributed to the fact that the amphiphilic SL can permeate through the nonpolar HFE domains, whereas Li⁺ and TFSA⁻ move only in the polar domains. This phenomenon is likely responsible for the rapid diffusion of SL, as observed in the experimental diffusivity data for the LHCEs, where $D_{\text{SL}}^{\text{self}} > D_{\text{Li}}^{\text{self}}$ (Figure 1a). Therefore, the presence of HFE results in faster dynamics, loosening the chain-like coordination structures and facilitating fragmentation. In the LHCEs, the Li⁺-ion exchange/hopping conduction is unlikely to occur with respect to the displacement of SL and TFSA⁻ in the chain-like coordination structures. Instead, the Li⁺-ion conduction mechanism is likely dominated by the translational motion of Li⁺ ions within the fragmented polar domains, some of which can be further isolated in the highly diluted LHCEs in the low c range of less than 1.57 mol dm^{-3} . These changes in the solution structure upon dilution with HFE are supported by the dynamic ion correlations shown in Figure 2, resulting in a decrease in $t_{\text{Li}}^{\text{EC}}$ in the high c region due to the reduced contribution of Li⁺ ions to the total ion conductivity as demonstrated by the decreased $\sigma_{+}^{\text{self}}/\sigma_{-}^{\text{self}}$ and $\sigma_{++}^{\text{distinct}}/\sigma_{-}^{\text{self}}$ and a further increase in $t_{\text{Li}}^{\text{EC}}$ in the low c region predominantly owing to the enhanced Li⁺-TFSA⁻ interaction.

4. CONCLUSIONS

The ion transport properties and solution structure in [Li(SL)₂][TFSA] diluted with HFE were investigated. Onsager transport coefficients were experimentally estimated based on concentrated-solution theory to elucidate the dynamic ion correlations. The value of $\sigma_{++}^{\text{distinct}}/\sigma_{-}^{\text{self}}$ significantly decreased in the low c range, suggesting that the excessive addition of HFE diminishes the unique Li⁺-ion exchange/hopping conduction and enhances the anti-correlated Li⁺-Li⁺ motions. The snapshots of MD simulations clearly illustrated the nano-segregated solution structure in SL-based LHCEs with polar and nonpolar bi-continuous domains. The fragmentation of the ion-conducting pathway was more pronounced at a higher HFE content, which is closely linked to the decrease in $\sigma_{++}^{\text{distinct}}/\sigma_{-}^{\text{self}}$. The MD simulations further

revealed the Li⁺-ion exchange/hopping conduction mechanism in the SL-based HCE. However, the presence of HFE likely resulted in faster dynamics, loosening the chain-like coordination structures and causing fragmentation. In the higher c range of $1.57\text{--}2.97 \text{ mol dm}^{-3}$, the unique coordination structure collapsed, which likely decreased the contribution of Li⁺ ions to the total ion conduction. This explanation is supported by the decreased $\sigma_{+}^{\text{self}}/\sigma_{-}^{\text{self}}$ and $\sigma_{++}^{\text{distinct}}/\sigma_{-}^{\text{self}}$, resulting in a decrease in the Li⁺ transference numbers. In the low c range of less than 1.57 mol dm^{-3} , further addition of HFE enhanced the Li⁺-TFSA⁻ interactions, thus increasing $t_{\text{Li}}^{\text{EC}}$ and decreasing ionic conductivity. Therefore, the degree of dilution should be optimized to maximize its effect on Li⁺-ion conductivity and salt diffusion coefficients. The highest value of $\sigma_{\text{ion}} \times t_{\text{Li}}^{\text{EC}}$ for the SL-based LHCEs was obtained at $c = 1.57 \text{ mol dm}^{-3}$ (Table S1). However, some limitations in the ion transport of SL-based LHCEs exist. Therefore, further studies on ion transport in LHCEs would be helpful in achieving a design principle for liquid electrolytes with high ionic conductivity and large $t_{\text{Li}}^{\text{EC}}$ values.

■ ASSOCIATED CONTENT

Supporting Information

The Supporting Information is available free of charge at <https://pubs.acs.org/doi/10.1021/acs.jpcc.3c02112>.

Plots of Li/Li⁺ electrode potential against the natural logarithm of Li⁺ concentration (c); salt concentrations and experimentally obtained transport parameters; normalized transport coefficients; atom type and partial charge on each atom in HFE; parameters for bond stretching, angle bending, and torsion angle potentials and nonbonded interactions of HFE; number of ions and molecules for MD simulations; concentration dependence of ionicity; dependence of the volume fraction of [Li(SL)₂][TFSA] on the transport coefficient $\sigma_{++}^{\text{distinct}}/\sigma_{-}^{\text{self}}$; radial distribution functions g around Li⁺ ions and integrated coordination numbers n , coordination number of oxygens within the first coordination shell around Li⁺ ion n^* ; and Raman spectra of [Li(SL)₂][TFSA]- x HFE at $700\text{--}770 \text{ cm}^{-1}$ (PDF)

■ AUTHOR INFORMATION

Corresponding Authors

Wataru Shinoda – *Research Institute for Interdisciplinary Science and Department of Chemistry, Okayama University, Okayama 700-8530, Japan*; orcid.org/0000-0002-3388-9227; Email: shinoda@okayama-u.ac.jp

Kazuhide Ueno – *Department of Chemistry and Life Science and Advanced Chemical Energy Research Centre (ACERC), Institute of Advanced Sciences, Yokohama National University, Yokohama 240-8501, Japan*; orcid.org/0000-0002-4684-5717; Email: ueno-kazuhide-rc@ynu.ac.jp

Authors

Taku Sudoh – *Department of Chemistry and Life Science, Yokohama National University, Yokohama 240-8501, Japan*

Shuhei Ikeda – *Department of Materials Chemistry, Nagoya University, Nagoya 464-8603, Japan*

Keisuke Shigenobu – *Department of Chemistry and Life Science, Yokohama National University, Yokohama 240-8501, Japan*

Seiji Tsuzuki – Advanced Chemical Energy Research Centre (ACERC), Institute of Advanced Sciences, Yokohama National University, Yokohama 240-8501, Japan;

orcid.org/0000-0001-8518-0300

Kaoru Dokko – Department of Chemistry and Life Science and Advanced Chemical Energy Research Centre (ACERC), Institute of Advanced Sciences, Yokohama National University, Yokohama 240-8501, Japan; orcid.org/0000-0002-9622-4345

Masayoshi Watanabe – Advanced Chemical Energy Research Centre (ACERC), Institute of Advanced Sciences, Yokohama National University, Yokohama 240-8501, Japan;

orcid.org/0000-0003-4092-6150

Complete contact information is available at:
<https://pubs.acs.org/10.1021/acs.jpcc.3c02112>

Author Contributions

[†]T.S. and S.I. equally contributed to this work.

Notes

The authors declare no competing financial interest.

ACKNOWLEDGMENTS

This study was supported in part by the Japan Society for the Promotion of Science (JSPS) KAKENHI (Grant Nos. 20H02837 and 22K19082 to K.U. and 19H05812 and 22H00340 to K.D.) and JST ALCA-SPRING (Grant Number JPMJAL1301), Japan. This study is also based on results obtained from a project, JPNP20004, subsidized by the New Energy and Industrial Technology Development Organization (NEDO). Calculations were performed on the supercomputer facilities of the Institute for Solid State Physics, the University of Tokyo, the Research Center for Computational Science, Okazaki, Japan (Project: 22-IMS-C108, 21-IMS-C106).

REFERENCES

- (1) Wu, F.; Maier, J.; Yu, Y. Guidelines and Trends for Next-Generation Rechargeable Lithium and Lithium-Ion Batteries. *Chem. Soc. Rev.* **2020**, *49*, 1569–1614.
- (2) Schmich, R.; Wagner, R.; Hörpel, G.; Placke, T.; Winter, M. Performance and Cost of Materials for Lithium-Based Rechargeable Automotive Batteries. *Nat. Energy* **2018**, *3*, 267–278.
- (3) Xu, K. Electrolytes and Interphases in Li-Ion Batteries and Beyond. *Chem. Rev.* **2014**, *114*, 11503–11618.
- (4) Yamada, Y.; Yamada, A. Review—Superconcentrated Electrolytes for Lithium Batteries. *J. Electrochem. Soc.* **2015**, *162*, A2406–A2423.
- (5) Yamada, Y.; Wang, J.; Ko, S.; Watanabe, E.; Yamada, A. Advances and Issues in Developing Salt-Concentrated Battery Electrolytes. *Nat. Energy* **2019**, *4*, 269–280.
- (6) Qian, J.; Henderson, W. A.; Xu, W.; Bhattacharya, P.; Engelhard, M.; Borodin, O.; Zhang, J.-G. High Rate and Stable Cycling of Lithium Metal Anode. *Nat. Commun.* **2015**, *6*, 6362.
- (7) McOwen, D. W.; Seo, D. M.; Borodin, O.; Vatamanu, J.; Boyle, P. D.; Henderson, W. A. Concentrated Electrolytes: Decrypting Electrolyte Properties and Reassessing Al Corrosion Mechanisms. *Energy Environ. Sci.* **2014**, *7*, 416–426.
- (8) Doi, T.; Shimizu, Y.; Hashinokuchi, M.; Inaba, M. Dilution of Highly Concentrated LiBF₄/Propylene Carbonate Electrolyte Solution with Fluoroalkyl Ethers for 5-V LiNi_{0.5}Mn_{1.5}O₄ Positive Electrodes. *J. Electrochem. Soc.* **2017**, *164*, A6412–A6416.
- (9) Liu, J.; Kaneko, T.; Ock, J.-Y.; Kondou, S.; Ueno, K.; Dokko, K.; Sodeyama, K.; Watanabe, M. Distinct Differences in Li-Deposition/Dissolution Reversibility in Sulfolane-Based Electrolytes Depending on Li-Salt Species and Their Solvation Structures. *J. Phys. Chem. C* **2023**, *127*, 5689–5701.
- (10) Dokko, K.; Watanabe, D.; Ugata, Y.; Thomas, M. L.; Tsuzuki, S.; Shinoda, W.; Hashimoto, K.; Ueno, K.; Umebayashi, Y.; Watanabe, M. Direct Evidence for Li Ion Hopping Conduction in Highly Concentrated Sulfolane-Based Liquid Electrolytes. *J. Phys. Chem. B* **2018**, *122*, 10736–10745.
- (11) Shigenobu, K.; Dokko, K.; Watanabe, M.; Ueno, K. Solvent Effects on Li ion Transference Number and Dynamic Ion Correlations in Glyme- and Sulfolane-Based Molten Li Salt Solvates. *Phys. Chem. Chem. Phys.* **2020**, *22*, 15214–15221.
- (12) Nakanishi, A.; Ueno, K.; Watanabe, D.; Ugata, Y.; Matsumae, Y.; Liu, J.; Thomas, M. L.; Dokko, K.; Watanabe, M. Sulfolane-Based Highly Concentrated Electrolytes of Lithium Bis-(trifluoromethanesulfonyl)amide: Ionic Transport, Li-Ion Coordination, and Li-S Battery Performance. *J. Phys. Chem. C* **2019**, *123*, 14229–14238.
- (13) Yanagi, M.; Ueno, K.; Ando, A.; Li, S.; Matsumae, Y.; Liu, J.; Dokko, K.; Watanabe, M. Effects of Polysulfide Solubility and Li Ion Transport on Performance of Li-S Batteries Using Sparingly Solvating Electrolytes. *J. Electrochem. Soc.* **2020**, *167*, No. 070531.
- (14) Ren, X.; Chen, S.; Lee, H.; Mei, D.; Engelhard, M. H.; Burton, S. D.; Zhao, W.; Zheng, J.; Li, Q.; Ding, M.; Schroeder, M.; Alvarado, J.; Xu, K.; Meng, Y. S.; Liu, J.; Zhang, J. G.; Xu, W. Localized high-concentration sulfone electrolytes for high-efficiency lithium-metal batteries. *Chem* **2018**, *4*, 1877–1892.
- (15) Chen, S. R.; Zheng, J. M.; Mei, D. H.; Han, K. S.; Engelhard, M. H.; Zhao, W. G.; Xu, W.; Liu, J.; Zhang, J. G. High-Voltage Lithium-Metal Batteries Enabled by Localized High-Concentration Electrolytes. *Adv. Mater.* **2018**, *30*, No. 1706102.
- (16) Dokko, K.; Tachikawa, N.; Yamauchi, K.; Tsuchiya, M.; Yamazaki, A.; Takashima, E.; Park, J.-W.; Ueno, K.; Seki, S.; Serizawa, N.; Watanabe, M. Solvate Ionic Liquid Electrolyte for Li-S Batteries. *J. Electrochem. Soc.* **2013**, *160*, A1304.
- (17) Cao, X.; Jia, H.; Xu, W.; Zhang, J. G. Review-Localized High-Concentration Electrolytes for Lithium Batteries. *J. Electrochem. Soc.* **2021**, *168*, No. 010522.
- (18) Zhang, J. G.; Xu, W.; Xiao, J.; Cao, X.; Liu, J. Lithium Metal Anodes with Nonaqueous Electrolytes. *Chem. Rev.* **2020**, *120*, 13312–13348.
- (19) Cheng, L.; Curtiss, L. A.; Zavadil, K. R.; Gewirth, A. A.; Shao, Y.; Gallagher, K. G. Sparingly Solvating Electrolytes for High Energy Density Lithium-Sulfur Batteries. *ACS Energy Lett.* **2016**, *1*, 503–509.
- (20) Villaluenga, I.; Pesko, D. M.; Timachova, K.; Feng, Z.; Newman, J.; Srinivasan, V.; Balsara, N. P. Negative Stefan-Maxwell Diffusion Coefficients and Complete Electrochemical Transport Characterization of Homopolymer and Block Copolymer Electrolytes. *J. Electrochem. Soc.* **2018**, *165*, A2766–A2773.
- (21) Woolf, L. A.; Harris, K. R. Velocity Correlation Coefficients as An Expression of Particle-Particle Interactions in (Electrolyte) Solutions. *J. Chem. Soc., Faraday Trans. 1* **1978**, *74*, 933–947.
- (22) Dong, D.; Sälzer, F.; Roling, B.; Bedrov, D. How Efficient is Li-Ion Transport in Solvate Ionic Liquids under Anion-blocking Conditions in a Battery? *Phys. Chem. Chem. Phys.* **2018**, *20*, 29174–29183.
- (23) Fuller, T. F.; Doyle, M.; Newman, J. Simulation and Optimization of The Dual Lithium Ion Insertion Cell. *J. Electrochem. Soc.* **1994**, *141*, 1–10.
- (24) Kashyap, H. K.; Annappureddy, H. V. R.; Raineri, F. O.; Margulis, C. J. How Is Charge Transport Different in Ionic Liquids and Electrolyte Solutions? *J. Phys. Chem. B* **2011**, *115*, 13212–13221.
- (25) Vargas-Barbosa, N. M.; Roling, B. Dynamic Ion Correlations in Solid and Liquid Electrolytes: How Do They Affect Charge and Mass Transport? *ChemElectroChem* **2020**, *7*, 367–385.
- (26) Sudoh, T.; Shigenobu, K.; Dokko, K.; Watanabe, M.; Ueno, K. Li+ Transference Number and Dynamic Ion Correlations in Glyme-Li Salt Solvate Ionic Liquids Diluted with Molecular Solvents. *Phys. Chem. Chem. Phys.* **2022**, *24*, 14269–14276.

- (27) Watanabe, Y.; Ugata, Y.; Ueno, K.; Watanabe, M.; Dokko, K. Does Li-ion Transport Occur Rapidly in Localized High-Concentration Electrolytes? *Phys. Chem. Chem. Phys.* **2023**, *25*, 3092–3099.
- (28) Zugmann, S.; Fleischmann, M.; Amereller, M.; Gschwind, R. M.; Wiemhöfer, H. D.; Gores, H. J. Measurement of Transference Numbers for Lithium Ion Electrolytes via Four Different Methods A Comparative Study. *Electrochim. Acta* **2011**, *56*, 3926–3933.
- (29) Wohde, F.; Balabajew, M.; Roling, B. Li+Transference Numbers in Liquid Electrolytes Obtained by Very-Low-Frequency Impedance Spectroscopy at Variable Electrode Distances. *J. Electrochem. Soc.* **2016**, *163*, A714–A721.
- (30) Shinoda, W.; Mikami, M. Rigid-Body Dynamics in The Isothermal-Isobaric Ensemble: A Test on The Accuracy and Computational Efficiency. *J. Comput. Chem.* **2003**, *24*, 920–930.
- (31) Ikeda, S.; Tsuzuki, S.; Sudoh, T.; Shigenobu, K.; Ueno, K.; Dokko, K.; Watanabe, M.; Shinoda, W. Lithium Ion Dynamics in Sulfolane-based Highly Concentrated Electrolyte. *J. Phys. Chem. C* **2019**, *123*, 14229–14238.
- (32) Martínez, L.; Andrade, R.; Birgin, E. G.; Martínez, J. M. PACKMOL: A Package for Building Initial Configurations for Molecular Dynamics Simulations. *J. Comput. Chem.* **2009**, *30*, 2157–2164.
- (33) Andersen, H. C. Molecular Dynamics Simulations at Constant Pressure and/or Temperature. *J. Chem. Phys.* **1980**, *72*, 2384–2393.
- (34) Martyna, G. J.; Klein, M. L.; Tuckerman, M. Nosé–Hoover Chains: The Canonical Ensemble via Continuous Dynamics. *J. Chem. Phys.* **1992**, *97*, 2635–2643.
- (35) Ryckaert, J.-P.; Ciccotti, G.; Berendsen, H. J. C. Numerical Integration of The Cartesian Equations of Motion of a System with Constraints: Molecular Dynamics of n-Alkanes. *J. Comput. Phys.* **1977**, *23*, 327–341.
- (36) Martyna, G. J.; Tuckerman, M. E.; Tobias, D. J.; Klein, M. L. Explicit Reversible Integrators for Extended Systems Dynamics. *Mol. Phys.* **1996**, *87*, 1117–1157.
- (37) Tuckerman, M.; Berne, B. J.; Martyna, G. J. Reversible Multiple Time Scale Molecular Dynamics. *J. Chem. Phys.* **1992**, *97*, 1990–2001.
- (38) Hung, P. K.; Vinh, L. T.; Nghiep, D. M.; Nguyen, P. N. Computer Simulation of Liquid Al₂O₃. *J. Phys. Condens. Matter* **2006**, *18*, 9309.
- (39) Hayamizu, K.; Aihara, Y.; Arai, S.; Martinez, C. G. Pulse-Gradient Spin-Echo 1H, 7Li, and 19F NMR Diffusion and Ionic Conductivity Measurements of 14 Organic Electrolytes Containing LiN(SO₂CF₃)₂. *J. Phys. Chem. B* **1999**, *103*, 519–524.
- (40) Watanabe, M.; Nagano, S.; Sanui, K.; Ogata, N. Estimation of Li+ Transport Number in Polymer Electrolytes by The Combination of Complex Impedance and Potentiostatic Polarization Measurements. *Solid State Ionics* **1988**, *28-30*, 911–917.
- (41) Bruce, P. G.; Evans, J.; Vincent, C. A. Conductivity and Transference Number Measurements on Polymer Electrolytes. *Solid State Ionics* **1988**, *28-30*, 918–922.
- (42) Shigenobu, K.; Shibata, M.; Dokko, K.; Watanabe, M.; Fujii, K.; Ueno, K. Anion Effects on Li Ion Transference Number and Dynamic Ion Correlations in Glyme–Li Salt Equimolar Mixtures. *Phys. Chem. Chem. Phys.* **2021**, *23*, 2622–2629.
- (43) Piao, N.; Ji, X.; Xu, H.; Fan, X.; Chen, L.; Liu, S.; Garaga, M. N.; Greenbaum, S. G.; Wang, L.; Wang, C.; He, X. Countersolvent Electrolytes for Lithium-Metal Batteries. *Adv. Energy Mater.* **2020**, *10*, No. 1903568.
- (44) Cao, X.; Gao, P.; Ren, X.; Zou, L.; Engelhard, M. H.; Matthews, B. E.; Hu, J.; Niu, C.; Liu, D.; Arey, B. W.; et al. Effects of Fluorinated Solvents on Electrolyte Solvation Structures and Electrode/electrolyte Interphases for Lithium Metal Batteries. *Proc. Natl. Acad. Sci. U. S. A.* **2021**, *118*, No. e2020357118.
- (45) Saito, S.; Watanabe, H.; Ueno, K.; Mandai, T.; Seki, S.; Tsuzuki, S.; Kameda, Y.; Dokko, K.; Watanabe, M.; Umehayashi, Y. Li + Local Structure in Hydrofluoroether Diluted Li-Glyme Solvate Ionic Liquid. *J. Phys. Chem. B* **2016**, *120*, 3378–3387.
- (46) Perez Beltran, S.; Cao, X.; Zhang, J.-G.; Balbuena, P. B. Localized High Concentration Electrolytes for High Voltage Lithium–Metal Batteries: Correlation between the Electrolyte Composition and Its Reductive/Oxidative Stability. *Chem. Mater.* **2020**, *32*, 5973–5984.
- (47) Brouillette, D.; Irish, D. E.; Taylor, N. J.; Perron, G.; Odziemkowski, M.; Desnoyers, J. E. Stable Solvates in Solution of Lithium Bis(trifluoromethylsulfone)imide in Glymes and Other Aprotic Solvents: Phase Diagrams, Crystallography and Raman Spectroscopy. *Phys. Chem. Chem. Phys.* **2002**, *4*, 6063–6071.
- (48) Seo, D. M.; Borodin, O. A.; Han, S. D.; Boyle, P. D.; Henderson, W. A. Electrolyte Solvation and Ionic Association II. Acetonitrile-Lithium Salt Mixtures: Highly Dissociated Salts. *J. Electrochem. Soc.* **2012**, *159*, A1489–A1500.
- (49) Umehayashi, Y.; Mitsugi, T.; Fukuda, S.; Fujimori, T.; Fujii, K.; Kanzaki, R.; Takeuchi, M.; Ishiguro, S.-I. Lithium Ion Solvation in Room-Temperature Ionic Liquids Involving Bis-(trifluoromethanesulfonyl) Imide Anion Studied by Raman Spectroscopy and DFT Calculations. *J. Phys. Chem. B* **2007**, *111*, 13028–13032.
- (50) Humphrey, W.; Dalke, A.; Schulten, K. VMD: Visual Molecular Dynamics. *J. Mol. Graph.* **1996**, *14*, 33–38.

Recommended by ACS

Design of Localized High-Concentration Electrolytes via Donor Number

Juner Chen, Jianhui Wang, et al.

MARCH 10, 2023
ACS ENERGY LETTERS

READ 

Explore the Ionic Conductivity Trends on B₁₂H₁₂ Divalent Closo-Type Complex Hydride Electrolytes

Egon Campos dos Santos, Hao Li, et al.

JULY 26, 2023
CHEMISTRY OF MATERIALS

READ 

Discovery of the Li–Sr–La–Zr–O Compound and the Investigation of Its Lithium-Ion Conductivity

Kunimitsu Kataoka and Junji Akimoto

MAY 06, 2022
INORGANIC CHEMISTRY

READ 

Effect of Charge Non-Uniformity on the Lithium Dendrites and Improvement by the LiF Interfacial Layer

Yiwei You, Shunqing Wu, et al.

NOVEMBER 30, 2022
ACS APPLIED ENERGY MATERIALS

READ 

Get More Suggestions >